Published in final edited form as:
Proc SPIE. 2013 February 26; 8584: . doi:10.1117/12.2003976.

Stable Microwave Radiometry System for Long Term Monitoring of Deep Tissue Temperature

Paul R. Stauffer[*,a], **Dario B. Rodriques**[a], **Sara Salahi**[a], **Erdem Topsakal**[b], **Tiago R. Oliveira**[a], **Aniruddh Prakash**[a], **Fabio D'Isidoro**[a], **Douglas Reudink**[c], **Brent W. Snow**[c], and **Paolo F. Maccarini**[a]

[a]Radiation Oncology Dept., Duke University, Durham NC USA 27705

[b]Electrical and Computer Engineering Dept. Mississippi State University, Mississippi State, MS USA 39762

[c]Thermimage Corp., Taylorsville UT USA 84123

[d]Dept of Pediatric Urology, University of Utah, SLC UT USA

Abstract

Background—There are numerous clinical applications for non-invasive monitoring of deep tissue temperature. We present the design and experimental performance of a miniature radiometric thermometry system for measuring volume average temperature of tissue regions located up to 5cm deep in the body.

Methods—We constructed a miniature sensor consisting of EMI-shielded log spiral microstrip antenna with high gain on-axis and integrated high-sensitivity 1.35GHz total power radiometer with 500 MHz bandwidth. We tested performance of the radiometry system in both simulated and experimental multilayer phantom models of several intended clinical measurement sites: i) brown adipose tissue (BAT) depots within 2cm of the skin surface, ii) 3–5cm deep kidney, and iii) human brain underlying intact scalp and skull. The physical models included layers of circulating tissue-mimicking liquids controlled at different temperatures to characterize our ability to quantify small changes in target temperature at depth under normothermic surface tissues.

Results—We report SAR patterns that characterize the sense region of a 2.6cm diameter receive antenna, and radiometric power measurements as a function of deep tissue temperature that quantify radiometer sensitivity. The data demonstrate: i) our ability to accurately track temperature rise in realistic tissue targets such as urine refluxed from prewarmed bladder into kidney, and 10°C drop in brain temperature underlying normothermic scalp and skull, and ii) long term accuracy and stability of $\mp$0.4°C over 4.5 hours as needed for monitoring core body temperature over extended surgery or monitoring effects of brown fat metabolism over an extended sleep/wake cycle.

Conclusions—A non-invasive sensor consisting of 2.6cm diameter receive antenna and integral 1.35GHz total power radiometer has demonstrated sufficient sensitivity to track clinically significant changes in temperature of deep tissue targets underlying normothermic surface tissues for clinical applications like the detection of vesicoureteral reflux, and long term monitoring of brown fat metabolism or brain core temperature during extended surgery.

[*]paul.stauffer@duke.edu; phone 1 919 668-7419.

Keywords

Radiometry; non-invasive thermometry; brown adipose tissue metabolism; core temperature monitoring; vesicoureteral reflux detection

1. INTRODUCTION

There are numerous devices and techniques available to measure temperature deep in the body. Temperature may be recorded most accurately with invasive probes such as thermistors, thermocouples, or fiberoptic sensors that are placed interstitially into the target tissue or into natural body cavities such as the rectum, urethra, esophagus, ear or mouth [1, 2]. For many applications, invasive placement of probes directly into the desired tissue target is not clinically acceptable and there is no natural body cavity close enough for accurate estimates of target temperature. This is generally the case for temperature measurements of body organs and long term monitoring of subsurface tissue targets. For this purpose, there are a number of non-invasive thermometry approaches available including ultrasound backscatter, microwave radiometry, electrical impedance tomography (EIT), and magnetic resonance thermal imaging (MRTI)[3, 4]. Development continues on each of these approaches, with each showing clear advantages for specific clinical applications. To date, MRTI has demonstrated the best 3D spatial imaging of large tissue volumes with quite usable resolution and accuracy of better than 1°C in 1ml of tissue[5–8], but is suitable only for short term (<2 hours) monitoring due to cost and patient tolerance. For applications requiring long term monitoring of deep tissue temperature, a non-invasive method is desired that is tolerable and non-toxic to the patient,compact, portable, accurate to better than 1°C, and stable over long time periods that may last many hours, or in some applications, days.

This report describes one such approach, the use of passive microwave radiometry with a miniature microwave antenna sensor to be held securely in place on the skin under an elastic strap, or eventually an adhesive patch. The following sections briefly describe the radiometer sensor and readout electronics, phantom models used to evaluate the system, and radiometer performance in terms of accuracy and long term stability of deep tissue sensing.

2. METHODS

2.1 Radiometer

The basic components of our 500 MHz bandwidth 1.35 GH microwave radiometry system are shown in Figure 1. Several configurations of the radiometer front end electronics included inside the miniature radiometric sensor have evolved and specifics will be published elsewhere. Design considerations for one configuration have been described previously.[9] The radiometer consists of three basic components: i) a miniature skin contacting sensor with receive antenna and printed circuit with temperature references, RF switches, and initial application stage (+10–15db) of the extremely low level signal received from tissue, ii) an electronics chassis with additional amplification (+40db), filtering, and conversion to a digital signal proportional to received power in the selected passband of the filter, and iii) an analysis/processing software and computer display linked to the radiometer chassis by USB cable. The developed software provides critical signal processing with temporal averaging, compensation of drift in amplifier gain by cyclic comparison to known temperature references near the antenna, and calibration of the received power to equivalent tissue temperature conversion algorithm.

2.2 Antenna Sensor

Antennas were designed to maximize received energy from the desired deep tissue target (i.e. kidney, BAT depot, brain) and minimize power received from superficial tissues overlying the target. Thus sidelobes of the antenna radiation patterns were minimized in favor of more deeply penetrating central axis beam profile. Antenna designs were optimized with HFSS™ (Ansys Corp, Canonsburg PA) using target-specific tissue models with correct dielectric and thermal properties. The goals of optimization were: maximum energy collection from the deep target and minimum energy reflected at the antenna/skin interface. The diameter and height of antenna were constrained due to clinical practicality. Parameters available for adjustment in the optimization were: number of turns, substrate thickness, matching layer thickness, and dielectric properties. Thick substrate log spiral antennas were used as this geometry has been shown to offer higher directivity (more pronounced on axis beam profile).[10–12] Due to reciprocity, the pattern of energy collection from a receive antenna is identical to the power deposition pattern of that same antenna in transmit mode. Thus the distribution of received energy from antennas may be modeled as power deposition patterns and measured with Specific Absorption Rate (SAR) probes for validation of both antenna design and SAR simulation.

Optimum antenna size varies considerably for the range of intended clinical application. For sensing small temperature changes in kidney located 3–5cm below the skin for applications like detection of Vesicoureteral Reflux (VUR), 5 and 7 cm diameter log spirals have proven most appropriate.[10–12] For use in monitoring temperature of small targets like 1–2 cm dia depots of brown adipose tissue (BAT) within 2 cm of the skin surface, a smaller diameter antenna is required. Recent electromagnetic design efforts have optimized the radiation patterns of a miniature 2.6 cm diameter tapered log spiral antenna for use in sensing the temperature of brain tissue inside the cranium and also for sensing the high metabolic output of BAT deposits within 2cm of the tissue surface.[13] Figure 2A shows the design of a 5cm dia tapered log spiral for thick high dielectric constant ceramic substrate, and prototype radiometric sensor with combined 5cm antenna and printed circuit radiometer front end inside a copper shielding case. Figure 2B shows a 2.6cm dia tapered log spiral design and two functional prototypes, with an internal view of the radiometer printed circuit.

2.3 Evaluation Models

For this effort, we describe experimental models for testing radiometer performance in measuring the temperature of brain tissue inside the cranium, the temperature of urine inside a kidney or bladder, and the temperature of a small region of BAT located between layers of white fat and muscle tissues. From analysis of a de-identified patient head CT, we determined realistic values for the thickness of scalp, bone, and brain tissues for our physical model. Measurements showed that scalp thickness varies from 4.2mm (forehead) to 8mm (temporal lobe), and the skull bone was 6.7mm thick in both regions. Based on these dimensions, an experimental model of the human head was constructed around an artificial human skull (Life Size Skull, www.anatomywarehouse.com) with known geometry and dielectric properties similar to skull bone, and liquid phantom materials that mimic the properties of scalp and brain tissues. To model the thermodynamics of scalp which is a mixture of skin, muscle and fat tissues, an adjustable thickness (6–16mm) compartment was sealed against the outer surface of the skull and filled with circulating temperature-controlled distilled water ($\varepsilon_r = 74.2$, $\sigma = 0.28$ at 1.35 GHz). To simulate brain, a mixture of propylene glycol (46%) and deionized water (54%) was used to approximate the electrical properties of mixed grey and white matter ($\varepsilon_r = 52.43$, σ=1.45 S/m at 1.35 GHz). Dielectric properties of the tissue components were characterized using a coaxial dielectric probe (E85070C, Agilent Technologies, Santa Rosa CA) connected to a network analyzer (E5071C, Agilent Technologies) and adjusted to conform with Cole-Cole data for the

respective biological tissues.[14] The liquid brain phantom was circulated vigorously with a peristaltic pump through a latex balloon that filled the interior of the skull and temperature controlled with a heat exchanger to mimic changes in deep brain temperature resulting from anesthesia and subsequent thermoregulatory responses. Temperatures of the scalp and brain compartments were controlled independently to provide a range of different surface/deep temperature gradients for calibration of the temperature conversion algorithm, in order to distinguish volume averaged brain temperature from cooler and warmer scalp. The circulation velocity was a vigorous 1.7 liter/min in both liquid tissue phantoms to ensure homogeneous “brain” and “scalp” temperatures. A photograph of the experimental model is shown in Figure 3.

Similarly, a phantom model was constructed for evaluation of non-invasive sensing of urine temperature inside a kidney located at variable depth below layered fat and muscle tissues. The thermal and electrical properties of this radiometric monitoring situation are incorporated into the kidney model shown in Figure 4. In this model, the kidney target consists of a 10–50ml variable volume latex balloon sealed over the distal end of a Foley catheter. To create a differential temperature target, normal saline is circulated through the balloon and an external temperature-controlled heat exchanger. The kidney is positioned at variable distance (1–5cm) from a 0.010” thick Mylar film which replaces one side wall of a 25×25×15 cm Plexiglas box filled with vigorously circulated and temperature-controlled muscle tissue-equivalent material. The liquid muscle consists of a mixture of diethylene glycol (50%), deionized water (50%) and NaCl (<1%) to approximate the electrical properties of muscle (ε_r=52.4, σ=1.5 S/m at 1.35 GHz). This mixture was determined empirically as the best match to the Cole-Cole dispersion of muscle over the desired radiometric band (1.1–1.6 GHz) and has been reported previously.[11, 12] The liquid muscle was circulated vigorously with a peristaltic pump through the Plexiglas box and temperature-controlled heat exchanger to maintain constant temperature (e.g. 37°C). Temperatures of the kidney target and muscle environment were controlled independently to produce a range of surface/deep temperature gradients for determination of radiometer sensitivity as a function of target volume and temperature difference to surrounding muscle. The radiometric sensor was placed either in direct contact with the Mylar window at the left side of the Plexiglas box in Figure 4, or in contact with a 5mm thick layer of solid fat equivalent material located on the Mylar window. The mixture and properties for our fat tissue phantom have been reported previously.[11, 15]

Figure 4 also shows a diagram of the tissue model used for studies of brown adipose tissue. Physical realization of a BAT tissue model is similar in geometry to the kidney model just described. For measurements of a BAT tissue target at depth, the saline used to model urine is replaced with a BAT-equivalent liquid circulating in the same Foley balloon “target”. The liquid BAT-equivalent phantom consists of a mixture of 40% diacetin (glycerol diacetate), 59% deionized water and 1% NaCl to approximate the electrical properties of brown adipose tissue (ε_r=8.7, σ=2.6 S/m at 1.85 GHz). To model a small depot of BAT underlying white adipose tissue, the radiometric sensor was placed directly against the Mylar window and a layer of solid fat-equivalent phantom secured against the inside of the Mylar just above the BAT balloon target. As in the kidney model, the temperature of circulating muscle and BAT liquid materials was controlled separately to generate a differential target temperature.

3. RESULTS

3.1 Simulated Antenna Performance

Simulations of antenna radiation patterns were performed in realistic patient heterogeneous tissue models segmented from CT or MR scans, as well as in computer models of the experimental multilayer tissue phantom models. These simulations were used in the initial

antenna design stage to optimize received power from the tissue target for each clinical application. Simulations were also used to enable calibration of the algorithm that converts received power to equivalent target temperature, which is based on simulation of expected percentage of signal from the target, expected temperature distribution in subsurface tissue, and known (measured) antenna/skin interface temperature. Exemplary simulations of expected receive patterns are shown for monitoring: i) brain core temperature in an adult human patient, ii) “30ml kidney” target at 3 cm depth in muscle phantom from Figure 4A, and iii) a 6ml region of BAT located at depth between layers of white fat and muscle tissue in the model of Figure 4B.

Brain Core Temperature Monitoring—Figure 5 shows the SAR pattern of the 2.6cm dia tapered log spiral antenna as optimized for use in sensing brain temperature through scalp and skull, as simulated with HFSS at the center frequency of the radiometric band (1.35 GHz). While it is clear that the highest power is deposited superficially in the scalp, the simulations demonstrate significant power deposition (or received energy) from deep in brain. As expected there is little power deposited in the bone due to its low electrical conductivity. The simulations shown in Figure 6 further define the sensitivity of brain radiometry by stating the percentage of total energy received by the 2.6cm antenna that emanates from brain tissue inside the cranium. This efficiency of brain tissue monitoring is listed for three typical radiometric sense frequencies. It may be noted that the lower end of our current system receive band is actually less efficient at sensing brain temperature than the upper end of the band where 41% of the energy collected by the antenna comes from the brain. There is a tradeoff between increased loss from attenuation in tissue at higher frequencies and lower received power due to directivity as the antenna becomes smaller compared to the wavelength at lower frequencies. In practice, our radiometer system will collect a signal from deep brain that is a weighted average over all frequencies within the sensing bandwidth (1.1–1.6 GHZ).

Kidney Monitoring – VUR Detection Application—For sensing temperature rise deeper in the torso, a larger diameter spiral antenna may be used to collect more energy from depth. Figure 7 shows the SAR pattern of a 5cm dia tapered log spiral antenna looking into the kidney phantom model, as simulated with HFSS at the center frequency of the radiometric band (1.35 GHz). Again it is clear that the highest contribution to total received power is from superficial muscle tissue, but the simulations show significant received signal from the deep kidney target.

The Figure 8 chart displays the dependence of energy received by a 7cm dia log spiral antenna on both volume and depth of a kidney target in muscle, as simulated with HFSS at a center band frequency of 1.35GHz. The simulations show that up to 20% of the total energy collected by the surface antenna may be received from a large 60ml kidney volume if centered only 2.5cm below the skin surface. Conversely, only 2% of the total signal is derived from a smaller 20ml kidney target when centered 4cm deep beneath the surface.

Brown Adipose Tissue Monitoring—Figure 9 gives the HFSS simulated SAR pattern at 1.85 GHz for the 2.6cm dia spiral antenna directed into the BAT tissue model of Figure 4B. Because the dielectric loss characteristic of BAT is higher than overlying white fat, the SAR in the 6ml ellipsoidal BAT volume is significant even when located beneath 1 cm of white fat. The optimized operating frequency for this new antenna is 1.5–2.2 GHz: When compared to kidney, the optimum sense frequencies are higher since BAT depots are closer to the surface than kidney. See additional details of this simulated case by Rodriques et al.[13]

3.2 Measured Radiometer Performance

To demonstrate the sensitivity and long term stability of our miniature radiometer sensor, we studied the output of the radiometer into a known test load - the human scalp/skull/brain model of Figure 3 with separately controlled scalp and brain phantom temperatures. Figure 10 displays the result of radiometric monitoring of the life size head model for >4.5 hours. Over this time, the radiometric signal (black curve) did not exhibit any significant drift, correctly following the brain phantom temperature within ±0.4°C as it was reduced by 10°C for one hour and then returned back to initial temperature. The radiometer sensor was in direct contact with the scalp which was controlled at 32°C for the duration of the test. Although the radiometer is sensitive to scalp temperature which is constant for the entire 4.5 hours, the radiometer correlates very closely with the changing intracranial “brain” temperature. This is because the equivalent radiometric brain temperature is calculated based on the simulated ratio of radiometric power deriving from tissue inside the skull relative to total radiometric signal collected by the sensor, and known surface temperature of the scalp. The software algorithm accounts for the known distribution of received energy from scalp and brain tissues, and correctly calculates the change in brain temperature that must result given the constant scalp temperature. The difference between the temperature of circulating brain phantom as measured by fiberoptic sensors in the inlet and outlet ports of the circulating brain balloon and the calculated equivalent radiometric brain temperature remained less than ±0.4°C over the 4.5 hour experiment.

4. DISCUSSION AND CONCLUSIONS

This report gives an overview of recent developments in the miniaturization of microwave antennas and circuitry for constructing small lightweight radiometric sensors that can be used either for short or long term monitoring of temperature at moderate depths up to several cm in the body. Figures 3–4 summarize the construction of computational and experimental tissue models for three practical applications of microwave radiometry. Figures 5–9 present examples of electromagnetic simulations of power deposition in three deep tissue targets, which all demonstrate that a significant amount of energy can be received from small tissue volumes at depth using sensitive radiometers in the 1–2 GHz region. Finally, experimental measurements shown in Figure 10 confirm our ability to determine temperature of tissue targets buried below variable temperature layered tissues using a single frequency band compact radiometer, and to remove the effects of amplifier drift and instability that have plagued radiometric thermometry systems in the past. The ability to accurately read temperature at depth below tissues at other temperatures will be enhanced by use of multiple frequency bands, as discussed by a number of previous investigators.[16–24] But the promising current results encourage continued effort on software algorithms that calibrate radiometric sensor output to specific tissue loads and test conditions, and produce effective prediction of temperature at depth even from single frequency band radiometry.

This paper summarizes recent work to build and test a 1.1–1.6 GHz single band radiometry system for measuring volume average temperature of tissue targets at moderate depth in the body. Computer models and experimental phantom models are described for several clinical applications for this technology. Electromagnetic and thermal simulations demonstrate the feasibility of sensing thermal radiation from tissue sufficient to detect >1–2°C temperature rise at depths up to 5cm in just a few ml volume of living tissue. Current software with temporal averaging and drift correction provides a stable radiometric signal for accurate long term (≥5 hrs) monitoring of deep tissue temperature. These results demonstrate that passive microwave radiometry is now poised to emerge as an accurate and affordable noninvasive thermometry approach for short and long term monitoring of subsurface tissue temperature.

Acknowledgments

The authors would like to acknowledge support from NIH R21-DK092912. We would also like to recognize significant contributions from a diverse team originating from the University of Tromso, University of Rome Tor Vergata, University of L'Aquila, and University of Utah, as well as the encouragement and commercial support from Doug Turnquist at Thermimage Corporation. We would like to acknowledge software and hardware support from Ansys Corp, Agilent Technologies, National Instruments, Aviso, Aprel Laboratories, MiniCircuits, Avago, Triquint, and expert assistance from Don Pearce in the Duke University Machine Shop.

REFERENCES

[1]. Sneed, PK.; Stauffer, PR.; Li, G.; Sun, X.; Myerson, R. Hyperthermia. Vol. 74. Elsevier Saunders Co; Philadelphia: 2010.

[2]. Stauffer, PR. Thermal therapy techniques for skin and superficial tissue disease. SPIE Optical Engineering Press; Bellingham WA: 2000.

[3]. Dewhirst, M.; Das, S.; Stauffer, P.; Craciunescu, O.; Vujaskovic, Z.; Thrall, D. Hyperthermia. Vol. 21. Elsevier - Saunders; Philladelphia: 2012.

[4]. Wust P, Cho CH, Hildebrandt B, Gellermann J. Thermal monitoring: invasive, minimal-invasive and non-invasive approaches. International Journal of Hyperthermia. 2006; 22(3):255–62. [PubMed: 16754347]

[5]. Craciunescu O, Stauffer P, Soher B, et al. Accuracy of real time noninvasive temperature measurements using magnetic resonance thermal imaging in patients treated for high grade extremity soft tissue sarcomas. Medical Physics. 2009; 36(11):4848–58. PMCID2773239. [PubMed: 19994492]

[6]. Gellermann J, Hildebrandt B, Issels R, et al. Noninvasive magnetic resonance thermography of soft tissue sarcomas during regional hyperthermia: correlation with response and direct thermometry. Cancer. 2006; 107(6):1373–82. [PubMed: 16902986]

[7]. Stauffer PR, Craciunescu OI, Maccarini PF, et al. Clinical utility of magnetic resonance thermal imaging (MRTI) for realtime guidance of deep hyperthermia. 2009; 7181:OI-1–12.

[8]. Weihrauch M, Wust P, Weiser M, Nadobny J, Eisenhardt S, Budach V, Gellermann J. Adaptation of antenna profiles for control of MR guided hyperthermia (HT) in a hybrid MR-HT system. Medical Physics. 2007; 34(12):4717–25. [PubMed: 18196799]

[9]. Klemetsen O, Birkelund Y, Jacobsen SK, Maccarini PF, Stauffer PR. Design of Medical Radiometer Front-End for Improved Performance. Prog Electromagn Res B Pier B. 2011; 27:289–306. [PubMed: 21779411]

[10]. Arunachalam K, Maccarini P, De Luca V, Bardati F, Snow B, Stauffer P. Modeling the detectability of vesicoureteral reflux using microwave radiometry. Phys. Med. Biol. 2010; 55(18):5417–35. [PubMed: 20736499]

[11]. Arunachalam K, Maccarini P, De Luca V, Tognolatti P, Bardati F, Snow B, Stauffer P. Detection of vesicoureteral reflux using microwave radiometry-system characterization with tissue phantoms. IEEE Trans Biomed Eng. 2011; 58(6):1629–36. [PubMed: 21257366]

[12]. Stauffer, P.; Maccarini, P.; Arunachalam, K., et al. Microwave Radiometry for Non-Invasive Detection of Vesicoureteral Reflux (VUR) Following Bladder Warming. SPIE Press; Bellingham WA: 2011. PMCID:3409575

[13]. Rodriques D, Maccarini P, Salahi S, Oliveira T, Pereira P, Limao-Vieira P, Stauffer P. Numerical 3D modeling of heat transfer in human tissues for microwave radiometry monitoring of brown fat metabolism. Proc. of SPIE. 2013; 8754

[14]. Gabriel S, Lau RW, Gabriel C. The dielectric properties of biological tissues: III. Parametric models for the dielectric spectrum of tissues. Physics in Medicine and Biology. 1996; 41(11): 2271–93. [PubMed: 8938026]

[15]. Birkelund Y, Klemetsen O, Jacobsen SK, Arunachalam K, Maccarini P, Stauffer PR. Vesicoureteral reflux in children: a phantom study of microwave heating and radiometric thermometry of pediatric bladder. IEEE Trans Biomed Eng. 2011; 58(11):3269–78. [PubMed: 21900069]

[16]. Bardati F, Brown VJ, Tognolatti P. Temperature reconstructions in a dielectric cylinder by multi-frequency microwave radiometry. Journal of Electronic Waves and Applications. 1993; 7(11): 1549–71.

[17]. Hand JW, Van Leeuwen GMJ, Mizushina S, et al. Monitoring of deep brain temperature in infants using multi-frequency microwave radiometry and thermal modelling. Physics in Medicine and Biology. 2001; 46(7):1885–903. [PubMed: 11474932]

[18]. Jacobsen S, Stauffer P. Multi-frequency radiometric determination of temperature profiles in a lossy homogenous phantom using a dual-mode antenna with integral water bolus. IEEE Transactions on Microwave Theory and Techniques. 2002; 50(7):1737–46.

[19]. Jacobsen S, Stauffer P. Non-invasive temperature profile estimation in a lossy medium based on multi-band radiometric signals sensed by a microwave dual-purpose body-contacting antenna. International Journal of Hyperthermia. 2002; 18(2):86–103. [PubMed: 11911486]

[20]. Jacobsen S, Stauffer PR. Non-Parametric 1-D Temperature Restoration in Lossy Media Using Tikhonov Regularization on Sparse Radiometry Data. IEEE Transactions on Biomedical Engineering. 2003; 50(2):178–88. [PubMed: 12665031]

[21]. Jacobsen S, Stauffer PR. Can we settle with single-band radiometric temperature monitoring during hyperthermia treatment of chestwall recurrence of breast cancer using a dual-mode transceiving applicator? Physics in Medicine & Biology. 2007; 52(4):911–28. [PubMed: 17264361]

[22]. Mizushina S, Shimizu T, Sugiura T. Non-invasive thermometry with multi-frequency microwave radiometry. Frontiers of Medical and Biological Engineering. 1992; 4:129–133. [PubMed: 1510885]

[23]. Mizushina S, Shimizu T, Suzuki K, Kinomura M, Ohba H, Sugiura T. Retrieval of temperature-depth profiles in biological objects from multi-frequency microwave radiometric data. Journal of Electromagnetic Waves and Applications. 1993; 7(11):1515–48.

[24]. Ohba H, Kinomura M, Ito M, Sugiura T, Mizushina S. Multifrequency microwave radiometry for non-invasive thermometry using a new temperature profile model function. IEICE Transactions on Electronics. 1995; E78-C(8):1071–81.

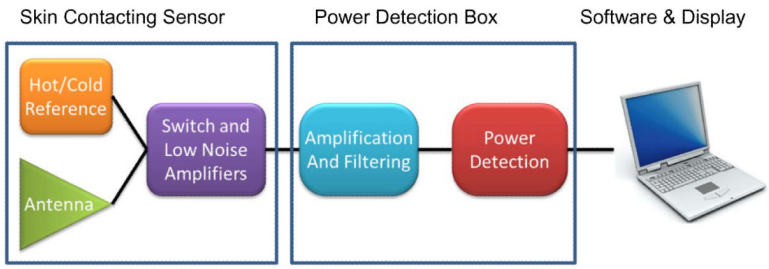

Figure 1.
Block diagram of basic components of 1.35 GHz single band radiometry system.

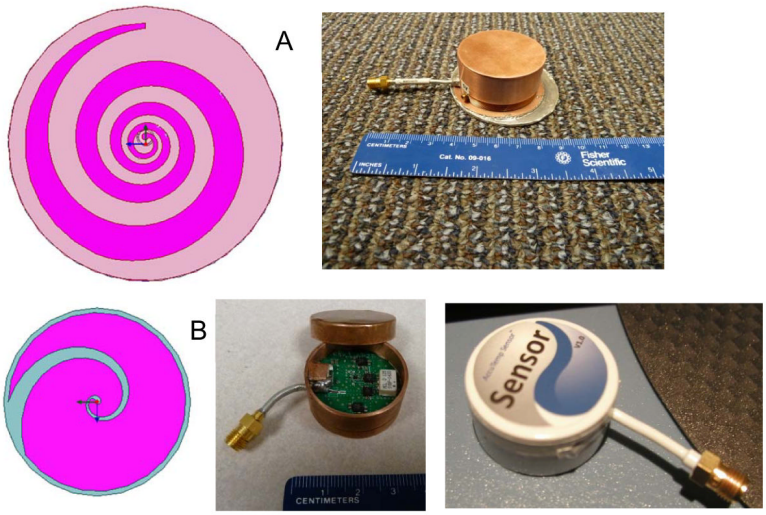

Figure 2.
Thick substrate deep penetrating tapered log spiral antenna designs and fabricated radiometric sensors with integrated antenna and radiometric first stage amplification. A) 5cm dia antenna sensor for monitoring bladder and kidney temperature, B) 2.6 cm dia antenna and sensor showing radiometer PCB with low noise amplifier, RF switches, and filters, and first clinical prototype for sensing brain temperature non-invasively via placement on the temple.

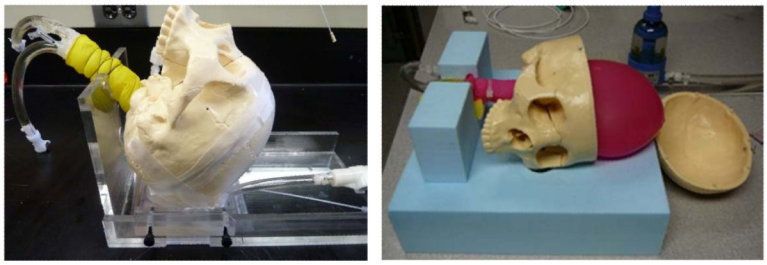

Figure 3.
Human head model with variable temperature brain tissue-equivalent liquid phantom circulating through a balloon that fills the inside of skull, and temperature controlled scalp tissue-equivalent liquid circulating through an adjustable thickness “scalp” under the skull. The black coax cable connects the external power detector and readout electronics to the radiometer sensor positioned under the model aiming up through the scalp and skull into brain.

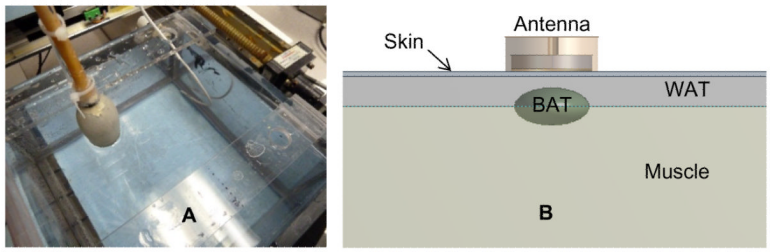

Figure 4.

A) Photo of experimental phantom model for determining radiometer sensitivity in a temperature-controlled variable volume “kidney” or “BAT” region located at variable depth in circulating muscle tissue-equivalent phantom at a separately controlled temperature. B) Diagram of associated computer model of variable size (2–6 ml) BAT region located beneath 1.5mm of skin and 1cm white fat tissue. The computer model was used during optimization of the antenna design to maximize received energy from a small sub-surface BAT depot. The experimental model was used to validate the computer simulation results and to quantify sensitivity of the radiometric sensors.

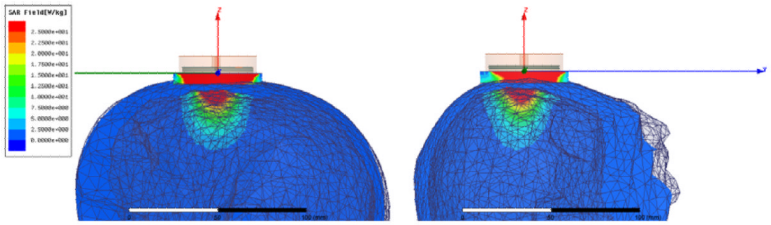

Figure 5.
HFSS simulated SAR pattern of a 2.6cm diameter log spiral microwave antenna on human head at the central radiometric frequency (1.35 GHz), demonstrating that although the radiometer is sensitive to scalp temperature, a significant portion of the microwave energy is received from brain tissue deep inside the cranium.

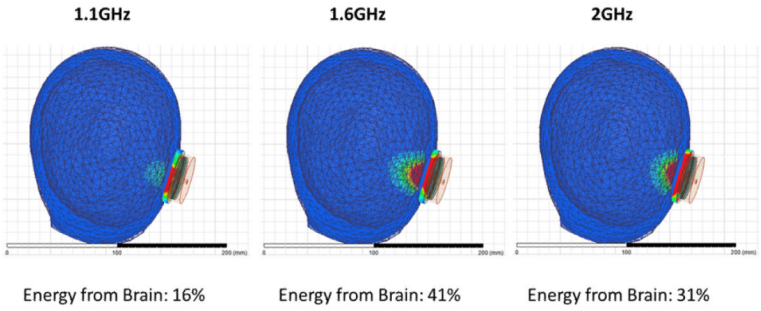

Figure 6.
shows the HFSS-simulated receive pattern for the 2.6cm directional beam log spiral antenna when placed on the heterogeneous multilayer human head model. The receive pattern is shown for three specific radiometric sensing frequencies from 1–2GHz. The radiometer tested in this work is sensitive primarily from 1.1 to 1.6 GHz. Note the low signal from skull, which is characterized by low dielectric constant and loss at microwave frequencies, and deep penetration of the field inside the skull.

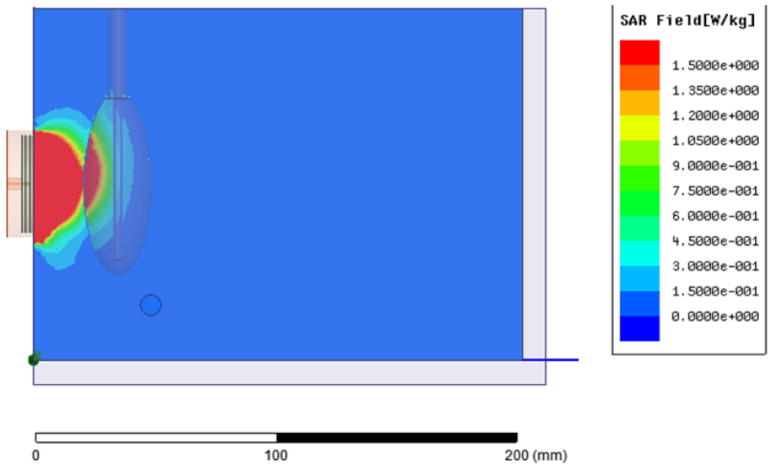

Figure 7.
HFSS simulation of receive pattern of 5 cm log spiral looking through Mylar window into the muscle and kidney phantom load, showing significant received energy from within the kidney (red) even when the center of kidney is 3 cm deep in muscle.

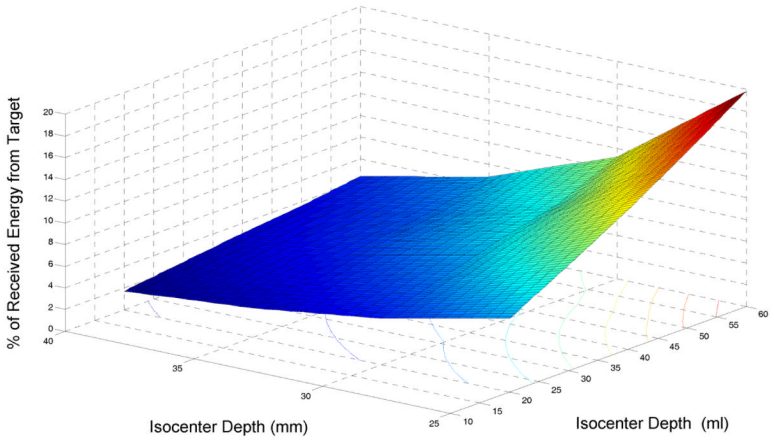

Figure 8.
HFSS simulated percentage of total SAR received by a 7cm dia surface antenna that originates from a urine target inside the kidney as a function of depth of the kidney isocenter and volume of urine in kidney

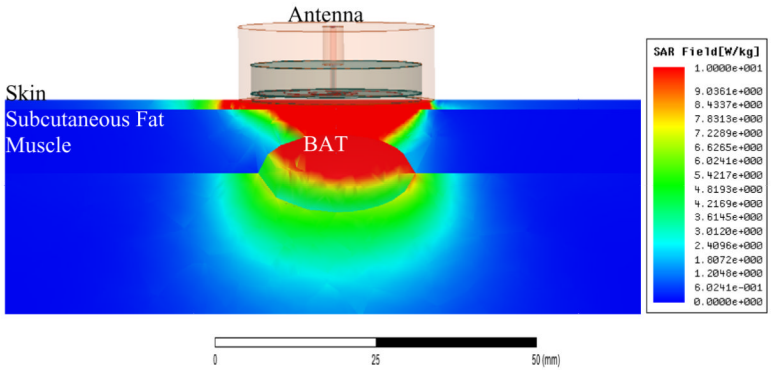

Figure 9.

HFSS simulation of SAR pattern of 2.6cm tapered log spiral directed into the layered tissue model of Figure 4B, demonstrating the ability to collect a significant portion of received signal from an elliptically shaped 6 ml depot of BAT embedded between white fat and muscle tissues.

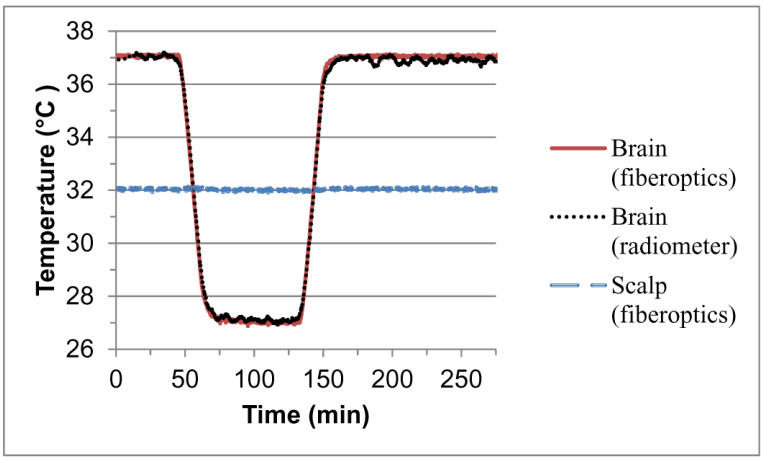

Figure 10.
Effective brain temperature derived from total power measurements of the non-invasive radiometric sensor (black curve) closely mirrors the actual temperature of circulating variable temperature brain phantom (red curve) as measured through constant temperature scalp (blue), with no significant measurement drift error over 4.5 hours of monitoring.